BULLETIN OF THE POLISH ACADEMY OF SCIENCES
TECHNICAL SCIENCES, Vol. 74(6), 2026, Article number: 6244
DOI: 10.24425/bpasts.2026.6244

Assessment of the feasibility of a semi-monolithic GaN VCSEL structure emitting at 450 nm based on electrical and thermal modeling

Robert P. SARZAŁA, Dominika DĄBRÓWKA*, and Hanna SADZEWICZ

Institute of Physics, Lodz University of Technology, Wólczańska 217/221, 93-005 Łódź, Poland

Abstract. This work presents a possible structure of a semi-monolithic GaN-based VCSEL with a tunnel junction, emitting at 450 nm and incorporating a nanoporous GaN (NP-GaN)/GaN distributed Bragg reflector (DBR). Self-consistent electrothermal simulations were performed to examine how the current-aperture radius and cavity length affect current-crowding and self-heating within the active region. Increasing the cavity length from 1λ to 10λ was found to markedly improve current uniformity and heat dissipation, while smaller apertures yielded lower maximum temperatures; a cavity length of 5λ combined with a 3 μm aperture radius was identified as the optimal design compromise. The influence of NP-GaN porosity on the thermal resistance of the rear DBR was further analyzed for two refractive-index models, linear and quadratic, while maintaining a target reflectivity above 99.98%. A porosity of about 30% offered the best trade-off between the number of required DBR pairs and thermal performance, giving a maximum device temperature of 317.1–317.6 K. Comparison with alternative AlInN/GaN and AlScN/GaN DBRs showed that the NP-GaN/GaN mirror achieves the lowest maximum temperature and requires fewer layer pairs, despite the technological challenges of controlling nanoporosity precisely. These findings provide guidance for designing thermally efficient, high-reflectivity DBRs for future GaN-based VCSELs.

Keywords: VCSEL; nanoporous GaN; DBR mirrors; computer simulations.

1. INTRODUCTION

The concept of the vertical-cavity surface-emitting laser (VCSEL) was first proposed in 1977, whereas the first commercially viable devices did not become available until the 1990s [1]. Today, the vertical-cavity surface-emitting laser (VCSEL) is one of the key radiation sources in modern optoelectronics. It is highly valued for its excellent beam quality, compact dimensions, low threshold current, and consequently low power consumption. Another important advantage is the possibility of processing and testing VCSEL structures directly at the semiconductor wafer level before device separation and packaging. Despite these advantages, commercially available VCSELs are currently based predominantly on GaAs material systems and, to a lesser extent, on InP, which restricts their operation primarily to the infrared spectral range. Therefore, the range of applications of these devices remains significantly limited.

Currently, the primary applications of VCSELs include displays, sensing, illumination, and optical communication. The development of GaN-based VCSELs could significantly expand these application areas by extending the accessible emission wavelength range into the visible spectrum and, potentially, even into the ultraviolet. Despite many years of intensive research, however, the development of commercially viable GaN-based VCSELs remains a major technological challenge, and no significant breakthrough has yet been achieved. One of the key obstacles is the fabrication of distributed Bragg reflectors (DBRs) with sufficiently high reflectivity to sustain laser operation while remaining lattice-matched to the GaN substrate and compatible with a single epitaxial growth process together with the laser active region. Such an approach would enable the realization of fully monolithic, or at least semi-monolithic, device structures.

In recent years, efforts have been made to achieve this type of structure using a technique that produces so-called nanoporous GaN (NP-GaN) [2], which, together with layers of conventional GaN, could form a high-reflectivity DBR mirror lattice-matched to the rest of the laser structure. The feasibility of employing NP-GaN/GaN mirrors in VCSELs has been confirmed experimentally. The first demonstrations involved optically pumped structures [3, 4], while further technological development led to the realization of electrically pumped GaN VCSELs with NP-GaN/GaN mirrors [5]. Researchers at Yale University have also demonstrated a room-temperature, electrically pumped c-plane GaN VCSEL employing a conductive NP-GaN/GaN mirror that enables vertical current injection through the structure [6].

Besides the design of the DBR mirror, current injection and spreading remain a critical issue in the development of GaN VCSELs. In conventional approaches, the current-spreading function can be performed by a transparent ITO layer, often combined with a dielectric SiO_2 current aperture. However, the presence of ITO within the optical cavity is associated with ad-

*e-mail: dominika.dabrowka@dokt.p.lodz.pl

Manuscript submitted 2026-07-06, revised 2026-09-10, initially accepted for publication 2026-09-11, published in November 2026.

© 2026 The Author(s). This is an open access article under the CC BY license (http://creativecommons.org/licenses/by/4.0/)

ditional absorption losses. An alternative solution is the use of a tunnel junction, which allows a highly doped n-GaN layer to be employed for effective current spreading while limiting the losses related to absorption in ITO [7]. The use of a buried tunnel junction additionally enables lateral confinement of the current flow, so that it can also function as a current aperture [8]. Tunnel junctions have already been successfully employed in electrically pumped GaN VCSELs, demonstrating the possibility of reducing the number of additional non-epitaxial layers and increasing the degree of structural integration [9, 10].

The combination of a tunnel junction with an NP-GaN/GaN mirror has also been realized experimentally. Studies conducted at the University of California, Santa Barbara (UCSB) demonstrated electrically pumped GaN VCSELs employing a bottom NP-GaN/GaN mirror together with a buried tunnel junction that confines the current-injection area [11]. This concept was subsequently developed further in long-cavity GaN VCSEL designs [12], confirming the feasibility of effectively integrating both solutions within a single laser structure.

The experimental demonstrations reported to date confirm the feasibility of realizing GaN VCSELs employing NP-GaN/GaN mirrors and tunnel junctions. Their further development, however, requires an appropriate choice of design parameters that accounts for the interplay between optical, electrical, and thermal phenomena. For NP-GaN/GaN mirrors, the degree of nanoporosity is of particular importance, as it affects both the refractive-index contrast and the number of DBR pairs required to achieve the target reflectivity, as well as the thermal conductivity of the layers. Increasing nanoporosity can therefore improve the optical properties of the mirror and reduce the required number of DBR pairs, while at the same time degrading the heat-dissipation capability of NP-GaN. The optimal degree of nanoporosity is thus not obvious and requires both effects to be considered.

Equally important is the choice of the device geometry itself. The cavity length and the size of the current aperture affect current spreading and the thermal conditions of the active region, and thus the degree of laser self-heating. Designing this type of VCSEL therefore requires incorporating both the geometrical parameters of the structure and the properties of the DBR mirror employed.

For this reason, the present work conducts a two-stage numerical analysis of a tunnel-junction GaN VCSEL emitting at a wavelength of 450 nm and incorporating a bottom NP-GaN/GaN mirror. The analysis was performed in two stages using computational modeling. First, the influence of the cavity length and the current-aperture radius on the uniformity of the current injected into the active region and on the temperature rise within the structure was investigated. On this basis, the device geometry was selected and subsequently kept constant in further calculations. Next, the effect of the degree of nanoporosity of the GaN layers on the thermal properties of the DBR mirror was analyzed while maintaining a high reflectivity. This made it possible to determine a mirror design offering a favorable trade-off between its optical and thermal properties. The results obtained were compared with alternative designs employing AlInN/GaN and AlScN/GaN mirrors [13].

2. STRUCTURE

Figure 1 shows the proposed semi-monolithic GaN-based VCSEL designed to emit at a wavelength of 450 nm. The device is fabricated on a GaN substrate bonded to a copper heat sink using a PbSn solder layer. The rear distributed Bragg reflector (DBR) consists of alternating NP-GaN and GaN layers, whereas the front DBR comprises eight pairs of dielectric SiO_2/TiO_2 layers. The active region consists of a single $In_{0.18}Ga_{0.82}N$ quantum well confined by two $In_{0.06}Ga_{0.94}N$ barrier layers. Its design is based on previously reported 450 nm light-emitting diode (LED) structures [14]. An InGaN tunnel junction and ion implantation forming the current aperture were incorporated into the device structure [14]. The electrical contacts were designed as ring-shaped gold contacts. Detailed parameters of individual structure layers, including their thickness and dopant concentrations, are summarized in Table 1.

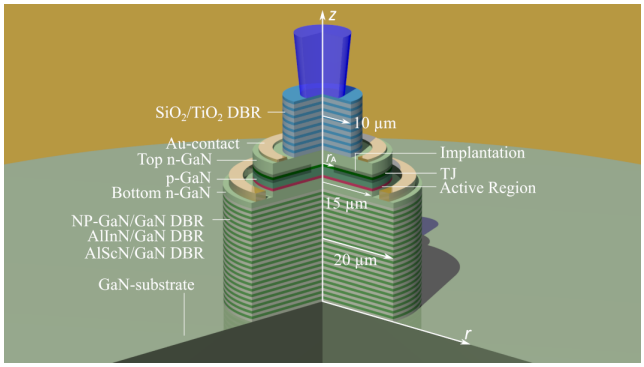

Fig. 1. Schematic of the proposed 450 nm GaN-based VCSEL employing an NP-GaN/GaN distributed Bragg reflector (DBR). Alternative designs of the rear DBR are also shown. The figure is not drawn to scale

The total cavity length was treated as a variable parameter. The preliminary electro-thermal results presented in this work cover cavity lengths ranging from 1λ to 10λ. An example of a 5λ cavity together with the corresponding standing-wave distribution is shown in Fig. 2. Varying the cavity length requires adjusting the thickness of the n-GaN layers. For shorter cavi-

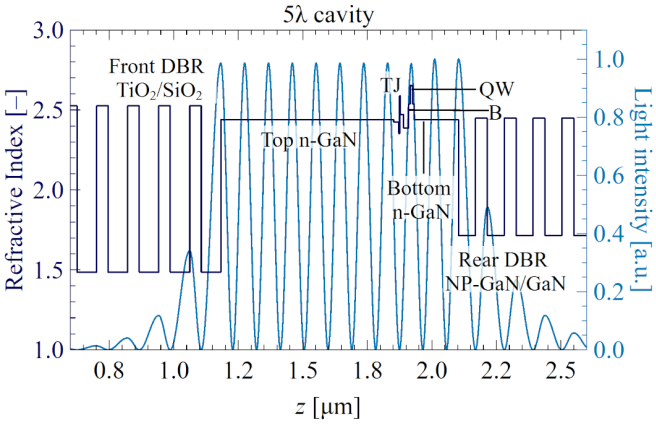

Fig. 2. Standing-wave distribution in the 5λ cavity overlaid on the refractive index profile of the entire VCSEL structure

Table 1
Design parameters of the modeled VCSEL laser. B – barrier, QW – quantum well, EBL – electron blocking layer

Layer		Material	Dopant concentration [cm^{-3}]	Thickness [nm]	
Front DBR	8×	TiO_2	–	44.5	
		SiO_2	–	75.8	
Top n-GaN		n-GaN	Si: 5.0×10^{18}	1.5λ	111.5
				5λ	665.3
				10λ	1588.3
		n-$In_{0.02}Ga_{0.98}N$	Si: 5.0×10^{19}	20	
Tunnel junction		n-$In_{0.21}Ga_{0.79}N$	Si: 2.0×10^{20}	3	
		p-$In_{0.21}Ga_{0.79}N$	Mg: 1.6×10^{20}	3	
		p-$In_{0.02}Ga_{0.98}N$	Mg: 1.0×10^{19}	12	
EBL		p-$Al_{0.13}Ga_{0.87}N$	Mg: 2.2×10^{19}	20	
Active region	B	$In_{0.06}Ga_{0.94}N$	–	5	
	QW	$In_{0.18}Ga_{0.82}N$	–	10.4	
	B	$In_{0.06}Ga_{0.94}N$	–	5	
Bottom n-GaN		n-GaN	Si: 5×10^{18}	1.5λ	80.7
				5λ	173.0
				10λ	173.0
Rear DBR		GaN	–	46	
		$Al_{0.83}In_{0.17}N$	–	50	
		$Al_{0.89}Sc_{0.11}N$	–	52	
		NP-GaN	–	See Fig. 3b	
Substrate		GaN	–	4×10^5	
Solder		PbSn	–	1×10^4	
Heat sink		Cu	–	5×10^6	

ties, the thicknesses of both the bottom and top n-GaN layers are reduced, whereas for longer cavities the increase in cavity length is achieved primarily by increasing the thickness of the top n-GaN layer.

3. NUMERICAL MODEL

The results presented here were obtained from numerical simulations performed using in-house models and a computer program developed by the Photonics Group of the Institute of Physics, Lodz University of Technology. The numerical models employed have previously been used to analyze thermal, electrical, and optical phenomena in various semiconductor laser structures [15, 16]. Their detailed description, together with the assumptions and material parameters adopted, is presented in [17].

In this work, a self-consistent thermal-electrical model was employed, enabling determination of the temperature and current-density distributions throughout the entire analyzed VCSEL structure. The electrical and thermal calculations are performed self-consistently, considering the temperature dependence of the material parameters. The electrical properties of the tunnel junction were incorporated into the model through an equivalent electrical conductivity of this region, determined based on the assumed contact resistivity of the junction. A value of $\rho_c = 1\times10^{-4}$ Ω·cm^2 was used in the calculations, consistent with the values reported in the literature [18] for the InGaN tunnel junction employed in our model.

The optical analysis, in turn, was used at the structure-design stage. It comprised one-dimensional calculations of the DBR mirrors, based on which the thicknesses of the individual layers were determined (see Table 1 and Fig. 3b), the number of DBR pairs required to achieve the target reflectivity (see Figs. 6 and 9), and the reflectance characteristics (see Figs. 7 and 8). For the resonant cavity, the analyzed thicknesses corresponded to successive multiples of the optical length for the designed emission wavelength (see Table 1).

To ensure comparability among the analyzed design variants, the supply voltage for each structure was adjusted to obtain the same average current density in the active region. This enables a direct relation between the observed differences in current and temperature distributions and changes in the device design parameters. The adopted approach thus enables a comparative assessment of the effect of design changes on the bottom DBR mirror (at a constant reflectivity) on the temperature rise inside the analyzed VCSEL.

The material parameters of the metals and dielectric materials used in the calculations were selected based on data available in the literature. These can be found in [17,19–21]. Table 2 presents the thermal conductivities that were specifically estimated for the purposes of this analysis. The perpendicular thermal conductivities of the NP-GaN material were estimated based on the formulas given in [22], while the parallel thermal conductivities were determined as a percentage of the thermal conductivity of

Table 2
Material parameters of the rear distributed Bragg reflectors (DBRs): $k_\perp$ – cross-plane thermal conductivity, $k_\parallel$ – in-plane thermal conductivity, and n_R – refractive index

Material		$k_\perp$ [W/(m·K)]	$k_\parallel$ [W/(m·K)]	Data sources	n_R [–]	Data sources
$Al_{0.83}In_{0.17}N$		4.87	4.87	[19]	2.252263	[24]
$Al_{0.89}Sc_{0.11}N$		8.00	8.00	[20,21]	2.154338	[13]
GaN		130.00	130.00	[23]	2.448112	[23]
NP-GaN	10%	25.00	117.00	[22]	See Fig. 3a	[25], [26]
	20%	21.25	104.00			
	30%	17.50	91.00			
	40%	13.75	78.00			
	50%	10.00	65.00			
	60%	6.25	52.00			
	70%	2.50	39.00			

monolithic GaN [23], with the percentage value resulting from the porosity of the material.

In addition, the design of the optical cavity and the estimation of the reflectivity of the investigated DBRs required the refractive indices of the constituent materials to be determined. For all rear DBRs considered in this study, the refractive indices were adopted from the literature: AlInN from [24], AlScN from [13], GaN from [23], and NP-GaN from [25, 26]. For nanoporous GaN (NP-GaN), the refractive index can be described by two relationships that account for the material porosity, φ. The first relationship is given by the quadratic expression [25, 26]:

$$n_{\mathrm{R,\,NP\text{-}GaN}} = \left((1-\varphi)\, n^2_{\mathrm{R,\,GaN}} + \varphi n^2_{\mathrm{R,\,air}} \right)^{1/2}, \tag{1}$$

whereas the second relationship is given by the linear expression [13]:

$$n_{\mathrm{R,\,NP\text{-}GaN}} = (1-\varphi)\, n_{\mathrm{R,\,GaN}} + \varphi n_{\mathrm{R,\,air}}, \tag{2}$$

where $n_{\mathrm{R,\,GaN}}$ and $n_{\mathrm{R,\,air}}$ denote the refractive indices of GaN and air, respectively.

Figure 3a shows the refractive index of NP-GaN calculated using both expressions as a function of the material porosity over the range from 10% to 70%. For both models, the refractive index of NP-GaN decreases with growing porosity. Moreover, the discrepancy between the values predicted by the quadratic and linear models becomes more pronounced as the porosity increases.

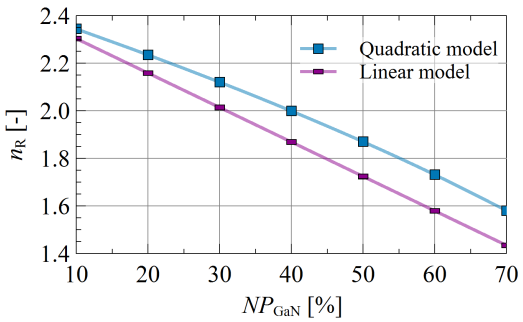

(a)

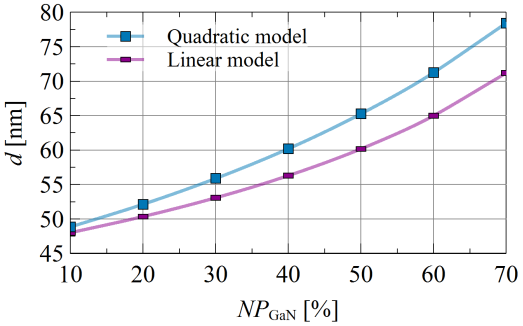

(b)

Fig. 3. Dependence of (a) the refractive index, n_R and (b) the NP-GaN layer thickness d on the GaN porosity for the quadratic (equation (1)) and linear (equation (2)) models

The change in the NP-GaN refractive index with porosity directly affects the required thickness of this layer in the DBR mirror. For each analyzed porosity value, the thickness of the NP-GaN layer was determined individually according to the quarter-wave condition:

$$d = \frac{\lambda}{4 n_R}, \tag{3}$$

with the calculations conducted for both refractive-index models considered. As shown in Fig. 3b, the decrease in refractive index with increasing porosity leads to an increase in the required NP-GaN layer thickness. The differences between the thicknesses determined for the two models likewise increase with increasing porosity. The NP-GaN layer thicknesses thus determined were subsequently considered in the further analysis of the DBR mirror properties.

4. RESULTS

An important aspect of VCSEL design is the proper selection of the device geometry to minimize the current-crowding effect. This phenomenon results from the non-uniform distribution of the injected current, leading to its concentration in localized regions of the device, typically near the edge of the current aperture. Consequently, the local current density increases, giving rise to excessive self-heating, non-uniform carrier injections, excitation of higher-order transverse modes, and, ultimately, degradation of the device performance.

Proper selection of the device dimensions, such as the diameter of the current aperture and the thicknesses of the spacer layers, which determine the cavity length while simultaneously providing current transport toward the active region, promotes a more uniform current distribution within the active region. As a result, thermal losses can be reduced, the emission characteristics improved, and the reliability and efficiency of the device enhanced. Therefore, minimizing the current-crowding effect is one of the key objectives in the optimization of the proposed VCSEL structure.

With these considerations in mind, the influence of the current-aperture radius and cavity length on the radial current density distribution in the active region of the proposed VCSEL structure was investigated. To facilitate comparison of the simulation results, the average current density in the active region was kept constant at 15 kA/cm^2. The simulation results obtained for three current-aperture radii (r_A = 2 μm, 3 μm, and 5 μm) and three cavity lengths (1.5λ, 5.0λ, and 10.0λ) are presented in Fig. 4.

For the shortest cavity (1.5λ, Fig. 4a), the current density distribution is markedly non-uniform, with a pronounced increase in current density near the edge of the current aperture. As the cavity length increases (Figs. 4b and 4c), the current distribution becomes progressively more uniform. For the 5.0λ cavity, the current-crowding effect is still present but is significantly reduced: the current density profile becomes flatter in the central part of the aperture, while the peak near the aperture edge becomes less pronounced. For the longest cavity (10.0λ, Fig. 4c),

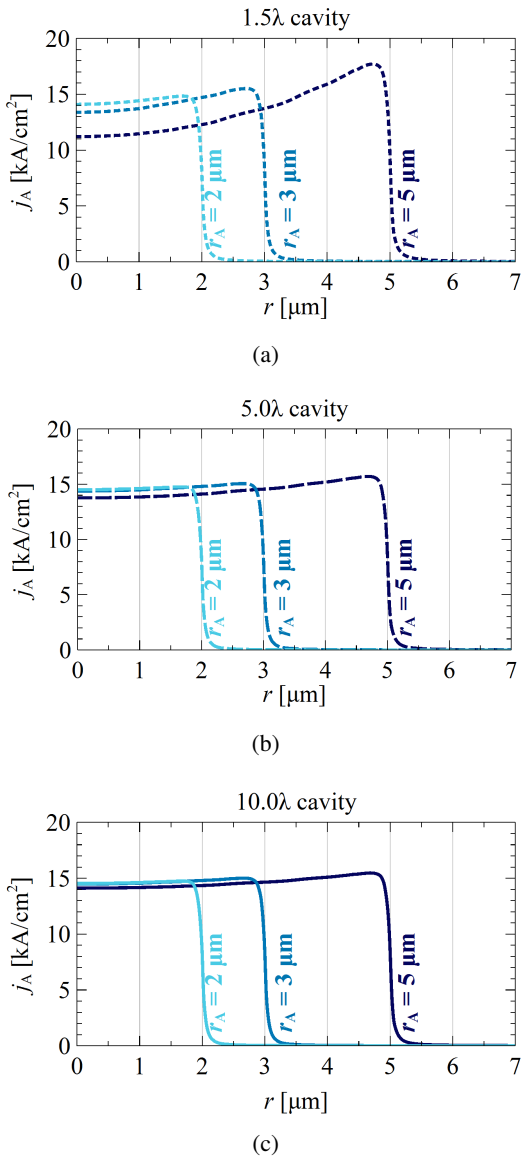

Fig. 4. Radial distribution of the current density, $j_A(r)$, injected into the active region of the VCSEL for three cavity lengths: (a) 1.5λ, (b) 5.0λ, and (c) 10.0λ. In each case, the results are shown for current-aperture radii of r_A = 2 µm, 3 µm, and 5 µm

the current density, j_A, is nearly uniform across the entire aperture, with only a slight increase near the aperture edge, confined to a narrow peripheral region.

The current-aperture radius primarily affects the position at which the current density drops to zero; however, for short cavities (1.5λ), it also has a noticeable influence on the shape of the current density profile. In particular, larger apertures (r_A = 5 µm) lead to greater current non-uniformity and a more pronounced increase in current density near the aperture edge. As the cavity length increases, the influence of the aperture radius gradually diminishes, and the current distribution becomes increasingly uniform. These results indicate that the cavity length is the primary factor governing the degree of current non-uniformity, whereas the aperture radius plays a significant role mainly in short-cavity VCSELs.

Having established the characteristics of the current density distribution and identified the factors governing the current-crowding effect, the analysis was extended to investigate the influence of the current-aperture radius and cavity length on the maximum temperature of the VCSEL structure. To this end, the maximum device temperature was evaluated as a function of cavity length over the range from 1λ to 10λ for the three current-aperture radii considered previously. The results are presented in Fig. 5.

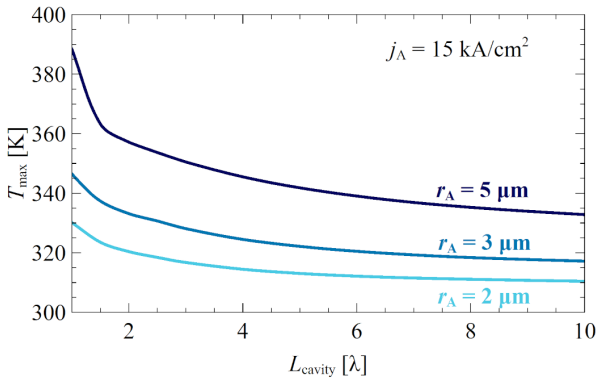

Fig. 5. Maximum temperature of the VCSEL structure as a function of cavity length for three current-aperture radii

The results shown in Fig. 5 reveal a clear dependence of the maximum device temperature on the cavity length. For all current-aperture radii considered, the maximum temperature decreases with increasing cavity length, owing to improved heat spreading within the cavity and, consequently, more efficient heat dissipation toward the heat sink. The temperature reduction is most pronounced for short cavities (from 1λ to approximately 4λ), beyond which the temperature gradually approaches a plateau. A comparison of the different current-aperture radii further shows that the lowest maximum temperature is obtained for the smallest aperture (2 µm), whereas the highest temperature is observed for the largest aperture (5 µm). Thus, increasing the current-aperture radius leads to an increase in the maximum device temperature, which can be attributed to the larger active-region volume and the corresponding increase in heat generation.

In summary, increasing the cavity length reduces the maximum device temperature, whereas smaller current apertures provide more favorable thermal conditions over the entire range investigated. However, beyond a certain cavity length, further extension yields only a marginal reduction in temperature, indicating diminishing thermal benefits. It should also be noted that longer cavities are associated with increased diffraction losses and facilitate the excitation of multiple longitudinal modes. Based on the analysis conducted, an aperture with a radius of 3 µm and a cavity length of 5λ were identified as suitable for the structure considered. This combination represents a compromise between mitigating the current-crowding effect and maintaining favorable thermal conditions within the device.

In addition to the parameters discussed above, the design of the DBR also has significant influence on the maximum tem-

perature within the VCSEL, as the heat generated in the active region is conducted through the rear DBR toward the heat sink. In the case of NP-GaN/GaN DBRs, the thermal properties are strongly dependent on the porosity of the nanoporous GaN layers (see Table 2). Two design strategies are commonly considered. The first aims to achieve high DBR reflectivity with the smallest possible number of layer pairs. This can be accomplished by employing materials with a large refractive-index contrast, which, in the case of NP-GaN/GaN DBRs, corresponds to highly porous NP-GaN layers. However, such structures exhibit relatively low thermal conductivity. The second strategy focuses on improving the thermal conductivity of the DBR by reducing the porosity of the NP-GaN layers and, consequently, the refractive-index contrast. The trade-off is that a larger number of DBR pairs is then required to maintain the same reflectivity, which may ultimately increase the overall thermal resistance of the reflector.

Figure 6 shows the influence of the NP-GaN layer porosity on the maximum device temperature and on the number of DBR pairs required to achieve a high reflectivity (R > 99.98%) for the linear and quadratic refractive-index models. In both cases, increasing the porosity reduces the number of DBR pairs required to achieve the target reflectivity because of the increasing refractive-index contrast between the DBR layers. However, the quadratic model requires a larger number of DBR pairs than the linear model, particularly at low porosities. For example, according to the quadratic model, increasing the porosity from 20% to 30% increases the maximum device temperature by only approximately 0.30 K, while reducing the required number of DBR pairs from 53.5 to 33.5. For the linear model, the corresponding increase in temperature is approximately 0.35 K, whereas the required number of DBR pairs decreases from 39.5 to 25.5. In contrast, increasing the porosity from 50% to 60% increases the maximum device temperature by approximately 2.9 K for the quadratic model and by approximately 2.6 K for the linear model, whereas the required number of DBR pairs is reduced only from 17.5 to 13.5 and from 14.5 to 11.5, respectively. These results indicate that the linear model enables high reflectivity to be achieved with fewer DBR pairs, particularly at

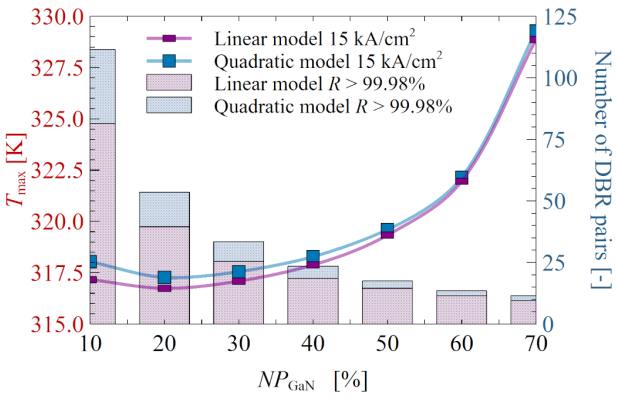

Fig. 6. Maximum device temperature, T_{max}, and the number of DBR pairs required to achieve a reflectivity of (R > 99.98%) as a function of the NP-GaN layer porosity for the linear and quadratic refractive-index models. The simulations were performed for a current density of 15 kA/cm^2

low and moderate porosities. Regardless of the refractive-index model, increasing the porosity degrades the thermal properties of the DBR, resulting in an increase in the maximum device temperature. For porosities up to approximately 40%, the temperature changes only slightly, whereas above 50% it increases rapidly. These results indicate that the optimal porosity range represents a compromise between minimizing the number of DBR pairs required to achieve high reflectivity and maintaining favorable thermal performance of the VCSEL.

In addition to reducing the number of required DBR pairs, increasing porosity also affects the shape of the mirrors' reflectance characteristics. Figure 7 shows the reflection spectra of GaN/NP-GaN structures for layer porosities of 20% and 30%. With increasing porosity, a marked broadening of the reflection band (stopband) is observed, while the maximum reflectance remains close to unity and the central wavelength remains unchanged at 450 nm. These results indicate that increasing porosity improves the spectral properties of the mirror, although, as shown by the analysis presented in Fig. 6, this comes at the cost of degraded thermal properties of the structure.

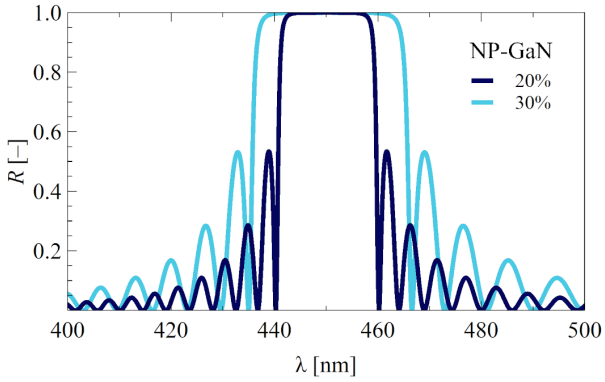

Fig. 7. Reflectance spectra of GaN/NP-GaN DBRs with NP-GaN layer porosities of 20% and 30%

The above analysis, however, does not account for additional optical losses that may occur in rear NP-GaN layers, arising, among other things, from light scattering at pores and structural inhomogeneities. To assess whether the presence of such losses could affect the determined trade-off between the optical and thermal properties of the mirror, additional calculations were performed incorporating an absorption coefficient in the NP-GaN layers. In this case, the introduction of absorption represents a simplified way of accounting for additional optical losses, without detailed modeling of the scattering mechanism.

Figure 8 shows the reflectivity of the DBR mirrors as a function of the number of pairs for NP-GaN porosities of 30% and 50% and various values of the absorption coefficient. For small absorption-coefficient values, on the order of a few cm^{-1}, the resulting dependences remain remarkably close to the lossless case. As the absorption increases, however, the maximum achievable DBR reflectivity becomes limited, an effect that is particularly pronounced for the lower NP-GaN porosity (30%). For large absorption values (100 cm^{-1}), the mirror reflectivity decreases, and increasing the number of pairs no longer leads to

a significant increase in reflectivity. It is worth noting that in this order of absorption in the DBR, the VCSEL laser is unlikely to have any chance of operating.

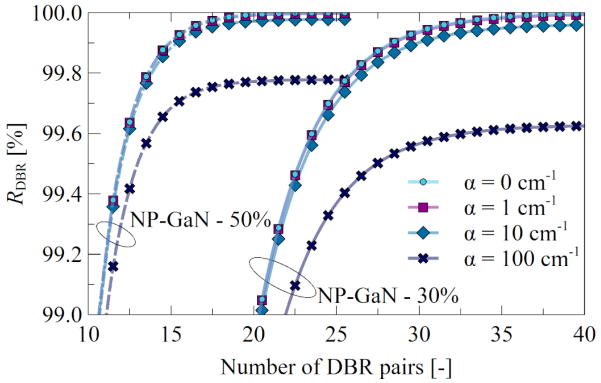

Fig. 8. Reflectivity of GaN/NP-GaN DBR mirrors as a function of the number of DBR pairs for NP-GaN porosities of 30% and 50% and absorption coefficients $\alpha = 0$, 1, 10, and 100 cm^{-1}

Based on the obtained results, an absorption coefficient of 10 cm^{-1} was adopted for further analysis, corresponding to relatively large additional optical losses for which a high DBR reflectivity can still be achieved, and the VCSEL laser could theoretically still operate. At the same time, the assumed reflectivity target was lowered, on account of absorption, to R > 99.94%. This made it possible to assess whether the conclusions drawn from the lossless analysis remain valid under less favorable optical conditions.

Figure 9 shows the maximum laser temperature and the number of DBR pairs required to achieve R > 99.94% as a function of NP-GaN porosity, for an absorption coefficient of 10 cm^{-1}. After accounting for the losses, the minimum of the considered optical-thermal trade-off shifts slightly toward a porosity of about 30%. This result indicates that the main conclusion of the analysis remains valid even after considering relatively large optical losses, i.e., a moderate NP-GaN porosity still provides a favorable trade-off between the number of required DBR pairs

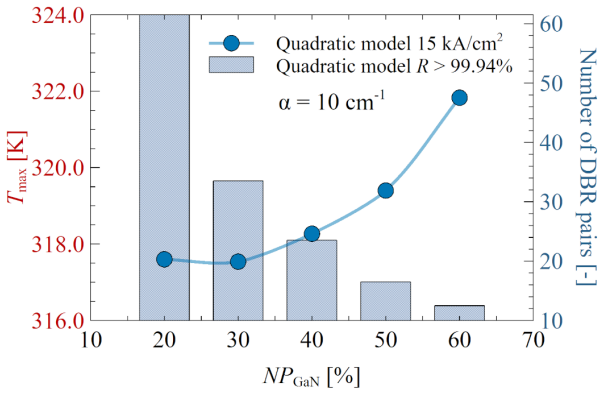

Fig. 9. Dependence of the maximum temperature T_{max} and the number of required DBR mirror pairs (for a reflectivity of R > 99.94%) on the porosity of the NP-GaN layer. Calculations performed for a current density of 15 kA/cm^2, a quadratic dependence of the refractive index on porosity, and considering absorption in the DBR equal to 10 cm^{-1}

and the maximum device temperature. In cases where the priority is to obtain the highest possible mirror reflectivity (with optical losses considered), higher porosities, on the order of 40–50%, may also be advantageous, as they provide a greater refractive-index contrast. It should be noted, however, that the actual magnitude of the optical losses may depend on the porosity and morphology of the NP-GaN layer, including the size, distribution, and uniformity of the pores, which can become problematic at high porosities. The final choice of porosity therefore requires appropriate technological control and optimization of the nanoporous GaN layer fabrication process. Nevertheless, the analysis performed indicates that accounting for additional optical losses does not change the fundamental conclusion regarding the favorable trade-off between the optical and thermal properties.

At the same time, it should be emphasized that the presented results are of a modeling nature. Both the assumed dependence of the refractive index on porosity and the actual level of optical losses in the NP-GaN layers may affect the achievable reflectivity and the number of DBR pairs required. The differences between the linear and quadratic models show that the way in which the optical properties of NP-GaN are described has a direct bearing on the design of very-high-reflectivity mirrors, and in particular on the number of pairs needed. For this reason, experimental verification of the obtained results is essential, including an assessment of the quality of the fabricated structures, the actual optical losses, and measurement of the mirror reflectivity for a specific number of DBR pairs. Only such a comparison will make it possible to determine which of the adopted models best describes the properties of the material under study and how many DBR periods are actually sufficient to achieve the required reflectivity.

The results indicate that the porosity of the NP-GaN layers should be selected as a compromise between achieving favorable optical properties and maintaining good thermal performance of the VCSEL. In both refractive-index models, increasing the porosity reduces the number of DBR pairs required to achieve high reflectivity and broadens the stopband. However, it also increases the maximum device temperature. A porosity of approximately 30% appears to provide the best compromise. For the quadratic model, this porosity results in a maximum device temperature of 317.6 K while reducing the required number of DBR pairs to 33.5. For the linear model, the corresponding values are 317.1 K and 25.5 DBR pairs, respectively. It should be noted, however, that fabricating NP-GaN layers with well-controlled porosity and producing high-quality DBRs may be technologically challenging. Therefore, an additional analysis was performed for VCSEL structures employing AlInN/GaN and AlScN/GaN DBRs, which currently represent the principal alternatives to NP-GaN/GaN reflectors.

A comparison with these alternative DBR structures showed that the lowest maximum device temperature was obtained for the NP-GaN/GaN DBR, reaching 317.6 K with 33.5 DBR pairs (see the left-hand side of Fig. 10). For the AlScN/GaN DBR (38.5 pairs, right-hand side of Fig. 10) and the AlInN/GaN DBR (58.5 pairs), the maximum temperatures increased to 325.1 K and 332.7 K, respectively. These results demonstrate that NP-

GaN/GaN DBRs enable the reduction in both the number of DBR pairs required to achieve high reflectivity and the maximum device temperature compared with the currently available alternative DBR designs.

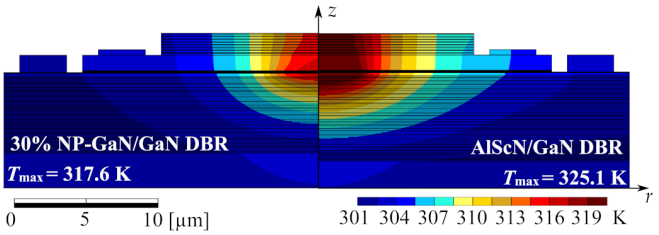

Fig. 10. Temperature distribution in the central (zr) cross-section of the VCSEL employing an NP-GaN/GaN DBR (left) and an AlScN/GaN DBR (right). Calculations performed for a current density of 15 kA/cm^2

It should be noted, however, that the DBR structures considered in this study differ substantially in terms of technological complexity. In particular, AlInN/GaN enables the fabrication of structures that are nearly lattice-matched to GaN, which promotes high epitaxial quality and reduces the formation of crystalline defects. In contrast, AlScN/GaN provides a high refractive-index contrast, but its implementation is associated with significant technological challenges, including difficulties in epitaxial growth, limited phase stability, and challenges in controlling the alloy composition and strain. In the case of NP-GaN/GaN DBRs, additional processing steps are required to produce the nanoporous layers. Moreover, precise control of the porosity and its uniformity remain challenging, and the porous structure may introduce significant optical scattering losses in the laser cavity.

5. CONCLUSIONS

The analysis performed showed that the device geometry significantly affects the current-density distribution and the thermal conditions in the semi-monolithic GaN VCSEL. In particular, for short cavities, a pronounced current-crowding effect is observed at the edge of the aperture, leading to increased non-uniformity of the current distribution. As the cavity length increases and the size of the active-region aperture is appropriately selected, this effect is weakened, and the current distribution becomes more uniform over the entire aperture area. At the same time, increasing the laser cavity length translates into improved thermal conditions and a lower maximum structure temperature. As a result, the optimal solution for the analyzed structure is a cavity length of about 5λ (further lengthening of the cavity leads only to a marginal improvement in the laser operating parameters) combined with an aperture radius of up to 3 μm.

The material properties, in particular the parameters of the DBR mirrors, in turn mainly determine the thermal conditions of the structure. The analysis performed showed that an NP-GaN porosity of about 30% represents the most favorable trade-off between the optical and thermal requirements. At this porosity, a DBR mirror reflectivity exceeding 99.98% can be achieved with a relatively small number of required pairs, depending on the adopted refractive-index model and amounting to about 33.5 for the quadratic model and 25.5 for the linear model. Considering additional optical losses in the NP-GaN layers does not fundamentally change this conclusion. For an absorption coefficient of $\alpha = 10$ cm^{-1} and a required reflectivity of R > 99.94%, a favorable optical-thermal trade-off is still obtained for a porosity of about 30%. For comparison, structures with AlScN/GaN and AlInN/GaN DBRs require about 38.5 and 58.5 pairs, respectively, while at the same time exhibiting a higher laser operating temperature. AlScN/GaN mirrors may therefore represent an alternative solution; however, their implementation is associated with technological challenges arising from the specific properties of AlScN.

ACKNOWLEDGEMENTS

This research was partially supported by the Polish Science Foundation under the TEAM NET FENG project (FENG.02.03-IP.05-0021/24). This work was completed while the second author was a PhD student at the Interdisciplinary Doctoral School of Lodz University of Technology, Poland.

REFERENCES

[1] K. Iga, "Surface-emitting laser-its birth and generation of new optoelectronics field," *IEEE J. Sel. Top. Quantum Electron.*, vol. 6, no. 6, pp. 1201–1215, 2000, doi: 10.1109/2944.902168.

[2] Y. Yao, Y. Liang, J. Guo, and H. Xiu, "The development and applications of nanoporous gallium nitride in optoelectronics: a review," *Semicond. Sci. Technol.*, vol. 38, no. 7, p. 74001, 2023, doi: 10.1088/1361-6641/accd14.

[3] S.-M. Lee, S.-H. Gong, J.-H. Kang, S.-W. Ryu, and Y.-H. Cho, "Optically pumped GaN vertical cavity surface emitting laser with high index-contrast nanoporous distributed Bragg reflector," *Opt. Express*, vol. 23, pp. 11023–11030, 2015, doi: 10.1364/OE.23.011023.

[4] S.M. Mishkat-Ul-Masabih, T.S. Luk, M. Monavarian, and D.F. Feezell, "Polarization-pinned emission of a continuous-wave optically pumped nonpolar GaN-based VCSEL using nanoporous distributed Bragg reflectors," *Opt. Express*, vol. 27, pp. 9495–9501, 2019, doi: 10.1364/OE.27.009495.

[5] S.M. Mishkat-Ul-Masabih, A.A. Aragon, M. Monavarian, T.S. Luk, and D.F. Feezell, "Electrically injected nonpolar GaN-based VCSELs with lattice-matched nanoporous distributed Bragg reflector mirrors," *Appl. Phys. Express*, vol. 12, p. 036504, 2019, doi: 10.7567/1882-0786/ab0576.

[6] R.T. ElAfandy, J.-H. Kang, B. Li, J.S. Kwak, and J. Han, "Room-temperature operation of c-plane GaN vertical cavity surface emitting laser on conductive nanoporous distributed Bragg reflector," *Appl. Phys. Lett.*, vol. 117, p. 011101, 2020, doi: 10.1063/5.0012281.

[7] C.-C. Shen *et al.*, "Design and fabrication of the reliable GaN based vertical-cavity surface-emitting laser via tunnel junction," *Crystals*, vol. 9, p. 187, 2019, doi: 10.3390/cryst9040187.

[8] S.-R. Jeon and G.M. Yang, "Vertical-surface-emitting diode using a GaN buried tunnel junction current aperture," *J. Korean Phys. Soc.*, vol. 41, pp. 1021–1024, 2002.

[9] S. Lee *et al.*, "GaN-based vertical-cavity surface-emitting lasers with tunnel junction contacts grown by metal-organic chemical vapor deposition," *Appl. Phys. Express*, vol. 11, p. 062703, 2018, doi: 10.7567/APEX.11.062703.

[10] C.A. Forman *et al.*, "Continuous-wave operation of m-plane GaN-based vertical-cavity surface-emitting lasers with a tunnel junction intracavity contact," *Appl. Phys. Lett.*, vol. 112, p. 111106, 2018, doi: 10.1063/1.5007746.

[11] N.C. Palmquist *et al.*, "Long-cavity M-plane GaN-based vertical-cavity surface-emitting lasers with a topside monolithic curved mirror," *Photonics*, vol. 10, p. 646, 2023, doi: 10.3390/photonics10060646.

[12] N.C. Palmquist *et al.*, "Characterization of long-cavity GaN vertical-cavity surface-emitting lasers with a topside dielectric lens," *Jpn. J. Appl. Phys.*, vol. 64, p. 050901, 2025, doi: 10.35848/1347-4065/add2b8.

[13] L. van Deurzen, T.-S. Nguyen, J. Casamento, H.G. Xing, and D. Jena, "Epitaxial lattice-matched AlScN/GaN distributed Bragg reflectors," *Appl. Phys. Lett.*, vol. 123, no. 24, p. 241104, 2023, doi: 10.1063/5.0176707.

[14] J. Slawinska, G. Muziol, A. Kafar, and C. Skierbiszewski, "Lateral Carrier Diffusion in Ion-Implanted Ultra-Small Blue III-Nitride MicroLEDs," *ACS Appl. Mater. Interfaces*, vol. 17, no. 4, pp. 6473–6479, 2025, doi: 10.1021/acsami.4c14784.

[15] D. Xu *et al.*, "Room-temperature continuous-wave operation of the In(Ga)As/GaAs quantum-dot VCSELs for the 1.3 µm optical-fibre communication," *Semicond. Sci. Technol.*, vol. 24, no. 5, p. 055003, 2009, doi: 10.1088/0268-1242/24/5/055003.

[16] M. Wasiak *et al.*, "Numerical model of capacitance in vertical-cavity surface-emitting lasers," *J. Phys. D: Appl. Phys.*, vol. 49, no. 17, p. 175104, 2016.

[17] D. Dąbrówka and R.P. Sarzała, "Study on Bottom Distributed Bragg Reflector Radius and Electric Aperture Radius on Performance Characteristics of GaN-Based Vertical-Cavity Surface-Emitting Laser," *Materials*, vol. 17, no. 13, p. 3107, 2024, doi: 10.3390/ma17133107.

[18] C. Skierbiszewski *et al.*, "Nitride-based laser diodes grown by plasma-assisted molecular beam epitaxy," *Appl. Phys. Express*, vol. 11, p. 034103, 2018, doi: 10.7567/APEX.11.034103.

[19] H. Tong, J. Zhang, G. Liu, J.A. Herbsommer, G.S. Huang, and N. Tansu, "Thermoelectric properties of lattice-matched AlInN alloy grown by metal organic chemical vapor deposition," *Appl. Phys. Lett.*, vol. 97, no. 11, p. 112105, 2010, doi: 10.1063/1.3489086.

[20] Y. Song *et al.*, "Thermal Conductivity of Aluminum Scandium Nitride for 5G Mobile Applications and Beyond," *ACS Appl. Mater. Interfaces*, vol. 13, no. 16, pp. 19031–19041, 2021, doi: 10.1021/acsami.1c02912.

[21] G.A. Alvarez *et al.*, "Thermal conductivity enhancement of aluminum scandium nitride grown by molecular beam epitaxy," *Mater. Res. Lett.*, vol. 11, no. 12, pp. 1048–1054, 2023, doi: 10.1080/21663831.2023.2279667.

[22] T. Zhou *et al.*, "Thermal transport of nanoporous gallium nitride for photonic applications," *J. Appl. Phys.*, vol. 125, no. 15, p. 155106, 2019, doi: 10.1063/1.5083151.

[23] M. Kuc, R.P. Sarzała, and W. Nakwaski, "Thermal crosstalk in arrays of III-N-based Lasers," *Mater. Sci. Eng. B*, vol. 178, no. 20, pp. 1395–1402, 2013, doi: 10.1016/j.mseb.2013.08.013.

[24] G. Cosendey, J.-F. Carlin, N.A. K. Kaufmann, R. Butté, and N. Grandjean, "Strain compensation in AlInN/GaN multilayers on GaN substrates: Application to the realization of defect-free Bragg reflectors," *Appl. Phys. Lett.*, vol. 98, no. 18, p. 181111, 2011, doi: 10.1063/1.3586767.

[25] C. Zhang *et al.*, "Mesoporous GaN for Photonic Engineering-Highly Reflective GaN Mirrors as an Example," *ACS Photonics*, vol. 2, no. 7, pp. 980–986, 2015, doi: 10.1021/acsphotonics.5b00216.

[26] F. Lüßmann, M. Hoormann, J. Hartmann, F. Meierhofer, and A. Waag, "Distributed Bragg reflectors with porous GaN: Experimental assessment of effective medium approximations," *Appl. Phys. Lett.*, vol. 128, no. 19, p. 192108, 2026, doi: 10.1063/5.032417.